ACS APPLIED ELECTRONIC MATERIALS

pubs.acs.org/acsaelm Article

Full and In Situ Printing of Nanogenerators that Are Based on an Inherently Viscous Piezoelectric Polymer: An Effort to Minimize "Coffee Ring Effect" and Nonprinting Operations

Yunnan Fang,* Haiyang Zou, Song Peng, Gaoya Dong, and Manos M. Tentzeris

Cite This: *ACS Appl. Electron. Mater.* 2023, 5, 4157−4167 Read Online

ACCESS | Metrics & More | Article Recommendations | Supporting Information

ABSTRACT: Among various printing technologies for fabrication of electronic devices, microplotter printing and inkjet printing provide the best printing resolution. For inkjet printing, which is compatible with only low-viscosity inks, the "coffee ring effect" and time-/labor-consuming nonprinting operations are among the most that impose challenges to its applications for rapid and large-scale fabrication of electronic devices. When printing a flexible electronic device that tends to bend spontaneously, relocating an unfinished/undried workpiece for post-printing treatments usually causes ink diffusion, resulting in deteriorated printing resolution, nonuniformity, and defects. Taking the printing of a poly(vinylidene fluoride)- (PVDF-) based flexible nanogenerator as an example, this work utilized a high-viscosity compatible microplotter printer and a concentrated/viscous PVDF ink (which minimized the "coffee ring effect)" and an in situ fabrication process (which not only maximally facilitated and minimized the nonprinting operations but also avoided the deterioration of the printing resolution and the nonuniformity/defects). A morphological comparison investigation showed that a PVDF patch printed (for only two passes with a concentrated 7 wt % PVDF ink) with a microplotter was morphologically homogeneous with no observable defects, while a PVDF patch printed (for 80 passes with a diluted 0.5 wt % PVDF ink) with a typical inkjet printer exhibited conspicuous nonuniformity and defects like grooves, pits, and cracks. Performance characterization of such a nanogenerator showed that it generated negative−positive twin pulses of short-circuit current during its cyclic bending and unbending, with a short-circuit current density magnitude up to ~0.4 μA/cm^2. A flexible carbon nanotube-based chemiresistive gas sensor was also fully printed in situ, in order to demonstrate that the in situ printing method utilized in this work is also compatible with fine features and low-viscosity inks.

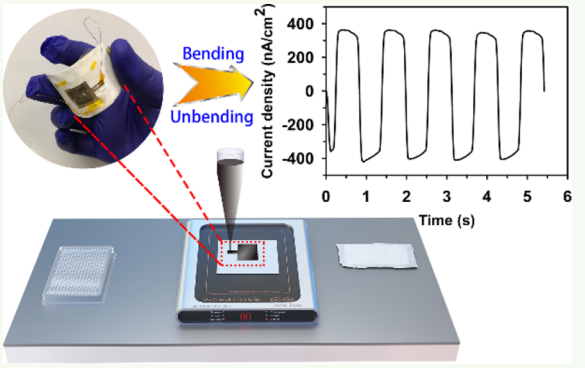

KEYWORDS: *in situ printing, coffee ring effect, poly(vinylidene fluoride), piezoelectric, flexible electronics, nanogenerator*

1. INTRODUCTION

Fabrication of electronic devices, especially for those designed for one-time or short-time use, via printing is receiving more and more attention by both the industry and the scientific community. Particularly, inkjet printing is probably the most commonly used for electronics fabrication due to its good combination of minimal waste, moderate cost, easy scaling-up, and great spatial resolution, deposition speed, and replicability. Inkjet printing, either alone or in combination with some other deposition technologies, has been utilized to fabricate a wide range of electronics such as solar cells,[1] light-emitting displays,[2] transistors,[3] and organic light-emitting diodes.[4] During the past decades, our group has inkjet printed a variety of multilayered and multicomponent electronic devices (such as gas[5−7] and strain[8,9] sensors, RF capacitors,[10] microfluidic devices,[11] and antennas[12]). Like most, if not all, inkjet printer users, we have been suffering from two drawbacks of inkjet printing: frequent interruptions by nonprinting operations (such as cartridge change, post-printing treatments, and a number of tedious processes associated with these activities) and nonuniformity/defects caused by the "coffee ring effect". In addition, when printing flexible electronics that tend to bend spontaneously, we have also been experiencing deteriorated printing resolution, nonuniformity, and defects caused by ink diffusion when relocating an undried workpiece for post-printing treatments.

A number of methods, such as addition of some cosolvents or surfactants to either slow solvent evaporation or create an opposing Marangoni flow[13,14] and utilizing solute particles with high aspect ratios,[15] have been reported to suppress the "coffee ring effect". Particularly, increasing the viscosity of the

Received: March 31, 2023
Accepted: July 24, 2023
Published: August 8, 2023

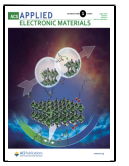

deposition fluid thus hindering the migration of the solute to the droplet edge has been shown to be a very efficient method to suppress the "coffee ring effect". For example, viscous hydrosoluble polymeric additives have been reported effective to facilitate uniform and ordered deposition of macroscale SiO_2 microspheres.[16] Addition of a viscous polymeric excipient (chitosan) to pharmaceutical solutions has been shown to efficiently facilitate the distribution homogeneity of the active pharmaceutical ingredients in dried films.[17] However, for some material-sensitive applications (such as sensing applications) in which any impurities should be avoided, a viscosity enhancer added to the ink, if not completely removed with a post-printing process, would negatively affect the performance of the resulting electronic devices. Besides, in order to enable proper droplet forming and jetting, an inkjet printer needs its ink to have a viscosity of no more than 20−40 cP depending on its density and surface tension,[18] which is an obstacle to reducing the "coffee ring effect" via viscosity increasing. When inkjet printing an ink containing an inherently viscous solute, the "coffee ring effect" often becomes more pronounced. Examples of inherently viscous materials include high molecular weight polymers, most ionic liquids, molecules with strong intermolecular hydrogen bonding (such as glycerol and glucose), and long-chain hydrocarbons. In order to meet the viscosity requirement of an inkjet printer, a low concentration has to be used when formulating an ink with an inherently viscous solute and consequently a huge number of passes have to be printed in order to achieve a desired working thickness. To prevent/minimize ink diffusion, a drying process has to be performed after a certain number of passes (typically three passes) have been printed, which normally makes the printing process prohibitively labor- and time-consuming and, more importantly, results in nonuniform/defective thin films (mainly due to the repeated taking place of the "coffee ring effect").

Poly(vinylidene fluoride) (PVDF), a piezoelectric polymer, is a typical example of inherently viscous materials. The viscosity of a 20 wt % PVDF (Solef 6010, MW 322 K) solution in *N*,*N*-dimethylformamide (DMF) was 790 cP (more than 60 times the recommended viscosity for a DMP-2800 series inkjet printer) and increased to 3860 cP when the PVDF concentration was increased to 30 wt %.[19] For a PVDF solution in RER 500 solvent (mainly butanone), while spin-coating normally uses 10 wt %, inkjet printing has to use a concentration of as low as 0.5 wt %, and even 1 wt % was too high.[20] PVDF or its copolymer with trifluoroethylene (PVDF-TrFE) has been traditionally deposited on a substrate surface with various patterned and unpatterned (full-surface) approaches such as spin coating,[21,22] electrospinning,[23−26] dip coating,[27] screen printing,[28,29] 3D printing,[30] and plotter printing.[31]

Mainly due to aggregation and clogging issues, the challenge to print with highly viscous inks is currently the largest technological hurdle for conventional inkjet and other nozzle-based printing technologies.[32,33] Two simple strategies seem to be able to allow a conventional inkjet printer to print viscous inks: One is to use large-diameter nozzles and the other to heat the ink at high temperatures. However, large-diameter nozzles result in low printing resolutions and a high temperature might degrade ink and cartridge components. Accordingly, it is desirable to have a printer that can print high-viscosity inks without sacrificing the printing resolution.

Among other types of printers for electronics fabrication, a typical microplotter is probably the only type that possesses a printing resolution comparable with that of a typical inkjet printer. However, in contrast to the numerous reports in the literature on using an inkjet printer for electronics fabrication, there are only a very limited number of reports on fabrication of electronics with a microplotter. Examples of microplotter printing include printing ZnO/Pt nanocomposite-based ink for chemoresistive gas sensors,[34] silver nanoparticle-based ink for organic thin film transistors (OTFTs),[35] and heteroliganded metal-based ink for "electronic olfaction" units.[36] One of the main advantages of a microplotter over an inkjet printer is its superior ability to print fluids with a wide range of viscosity. However, to the best of our knowledge, there have been no reports in the literature taking advantage of this feature of a microplotter to print inherently viscous materials.

In this work, we have demonstrated in situ fabrication of a multilayered and multicomponent PVDF-based nanogenerator with a microplotter, which maximally facilitated and minimized the nonprinting operations, minimized the "coffee ring effect", and avoided the deterioration of the printing resolution and the nonuniformity/defects resulted from workpiece relocating during the fabrication process. All the necessities needed for the fabrication were accommodated on the printer platen, and consequently, the workpiece never had to be moved throughout the entire fabrication process even though different inks and different post-printing treatments were involved. Different inks, even though used at different stages of the fabrication process, shared the same printhead. Compared with traditional inkjet printing, the in situ fabrication process described in this work circumvented a number of tedious and time-consuming nonprinting operations associated with cartridge changing and workpiece dislocation mentioned above. Different from previously reported methods in which impurities were added to the inks to increase their viscosity thus suppressing the " coffee ring effect", this work increased the ink viscosity by simply increasing the concentration of the functional material (PVDF). To the best of our knowledge, this work demonstrated the first fully printed PVDF-based nanogenerator. To demonstrate that the printing method employed in this work is also compatible with low-viscosity inks and fine features, a flexible carbon nanotube-based chemiresistive gas sensor was also fully printed in situ. The effort described in this work can help explore rapid and industrial-scale fabrication methods for electronic devices with great spatial resolution and reproducibility, minimal waste, and low cost.

2. EXPERIMENTAL SECTION

2.1. Screening for Solvent for PVDF Ink. A screening process, based on the Hansen solubility theory[37] (which is a way of predicting whether one material will dissolve in another to form a homogeneous solution), was performed for the first time to screen for the most appropriate solvent for a PVDF-based ink. The detailed theory and methodology based on which DMF was selected to dissolve PVDF will be described elsewhere in a separate report.

2.2. Ink Formulations. A 20 μg/mL single-walled carbon nanotube- (SWCNT-) based ink was made by immersing an appropriate amount of semiconducting SWCNT flakes (IsoNanotubes-S. NanoIntegris Technologies, Inc., Boisbriand, Quebec, Canada) in DMF and sonicating with a probe sonicator (Sonicator 3000, Misonix, Farmingdale, New York, USA), until a homogeneous suspension was obtained. A 10 mg/mL ink solution of 2-(2-hydroxy-1,1,1,3,3,3-hexafluoropropyl)-1-naphthol (SynQuest Laboratories, Inc., Alachua, Florida, USA) was prepared by dissolving an appropriate amount of this chemical in DMF solvent. DMF-based ink solutions containing 7 and 0.5 wt % of PVDF were made by dissolving an appropriate amount of PVDF powder (average MW ∼534,000; Sigma-Aldrich, St. Louis, Missouri, USA) in DMF solvent.

https://doi.org/10.1021/acsaelm.3c00428
ACS Appl. Electron. Mater. 2023, 5, 4157−4167

2.3. In Situ Printing of Electronic Devices with a Microplotter. Two types of electronic devices, a nanogenerator and a gas sensor, were printed in situ with a microplotter printer (GIX Microplotter II, SonoPlot Inc., Middleton, Wisconsin, USA). This printer, which used controlled ultrasonics to dispense picoliter volumes of fluid, was selected in this work due to its following advantages over a traditional inkjet printer:

(1) It is compatible with fluids with a viscosity of up to 450 cP. It turned out to print well with all the fluids (a homemade PVDF ink, a commercial silver nanoparticle ink, and DMF solvent) employed in this work.
(2) It can print droplets and true continuous lines/arcs with typical feature sizes of 20−50 and 5−200 μm with specific material combinations.
(3) Its large and open platen allows for the placement of a number of small equipment/items needed for the in situ fabrication of the nanogenerator and the gas sensor.
(4) Easy switching from one ink to another with no need for printhead change, thus eliminating tedious hassles like cartridge changing, drop offset setting, nozzle jetting testing, and realignments.

2.3.1. In Situ Printing of a PVDF-Based Nanogenerator. Figure 1 shows the necessities placed on the printer platen for the in situ fabrication of a PVDF-based nanogenerator (Figure 1a) and the step-by-step fabrication process (Figure 1b). A slim hot plate was placed at the center of the platen on which a piece of Teslin synthetic paper (with a thickness of 147 μm, PPG Industries, Pittsburgh, Pennsylvania, USA) was immobilized with heat-resistant Kapton tape. A 384-well microtiter plate was secured with double-sided tape on the left side of the platen to house the inks or DMF solvent. One well of the microtiter plate was filled with the homemade PVDF ink used for printing the PVDF patch, one well with the silver nanoparticle ink (EMD5730, Sun Chemical Corporation, Parsippany, New Jersey, USA) used for printing the silver electrodes, and six wells with DMF solvent used for washing the printhead when switching from one ink to the other. An absorbent pad was secured with double-sided tape on the right side of the platen to take the ink/solvent waste. A 60 μm aperture glass micropipette printhead (SonoPlot Inc., Middleton, Wisconsin, USA) was cut by 1 mm from the tapered end and mounted on the dispenser cartridge that was attached to the robotic positioner of the microplotter. The X, Y, and Z coordinates of some locations where the printhead needed to frequently access during the printing process were pre-stored in the computer system that controlled the positioner, so that the printhead was able to reach a particular position with only one click. Such locations included those of all the ink- or DMF-housing wells in the microtiter plate, the Teslin substrate, the starting points of printing, and the absorbent pad. Loading of an ink or a solvent into the printhead was realized by moving (either manually or computationally with the use of the pre-stored X/Y/Z coordinates) the printhead tip to a particular position where the tip was immersed in the ink or solvent solution. The ink or solvent would automatically rise up the inside of the glass printhead through capillary action. After the printing was done with one ink, the printhead was moved to the pre-stored location of the absorbent pad where the unused ink was sprayed out to empty the printhead, followed by three washes with DMF. In a typical washing cycle, the printhead was moved to one of the DMF wells in the microtiter plate to have the DMF solvent loaded and then moved to the absorbent pad to have the solvent sprayed out to empty the printhead. After the washing, the printhead was moved to the well housing the second ink to have the ink loaded there, followed by printing with this ink.

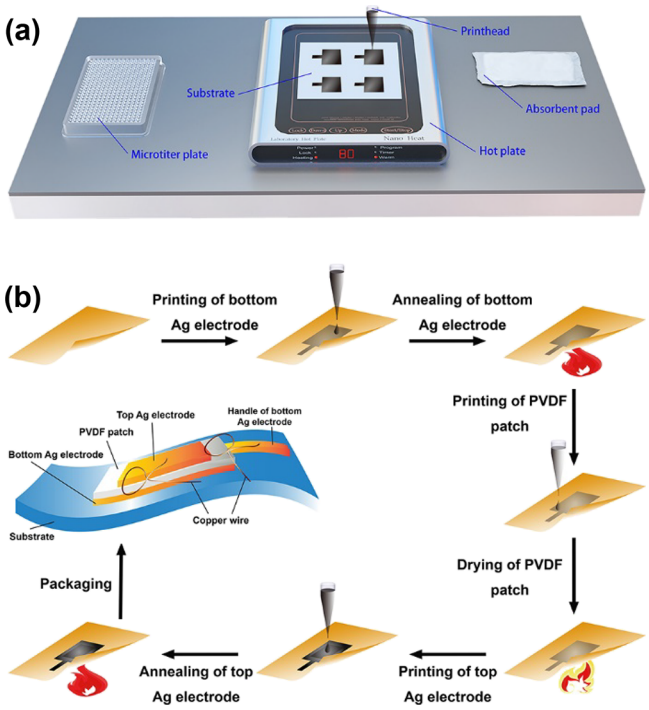

Figure 1. Schematics of in situ fabrication of a flexible piezoelectric nanogenerator that was based on pure PVDF. (a) Necessities placed on the printer platen for the fabrication of the nanogenerator. (b) Step-by-step fabrication process of the nanogenerator.

As shown in Figure 1b, to print a PVDF-based nanogenerator, the hot plate was heated to 45 °C. The bottom silver electrode, which was composed of a silver square patch (with dimensions of 1.5 cm × 1.5 cm) and a rectangle handle (0.75 cm × 0.3 cm), was printed for two passes with the silver nanoparticle ink on the Teslin substrate (12 cm × 7.5 cm). The newly printed bottom silver electrode was then subjected to an annealing process (150 °C/30 min) on the hot plate where the Teslin substrate rested. After the hot plate was cooled down to <60 °C, a PVDF patch (1.5 cm × 1.5 cm), which superposed the previously printed silver patch, was printed for two passes with the PVDF ink and then dried on the hot plate at 60 °C for 30 min. Finally, the top silver electrode patch (1 cm × 1 cm) was printed for two passes on the dried PVDF patch followed by annealing at 150 °C for 30 min on the hot plate. The top silver electrode (1 cm × 1 cm) was designed to be a little smaller than the PVDF patch (1.5 cm × 1.5 cm) in order to minimize the risk of circuit shorting caused by the direct contact of the bottom and the top silver patches. Two soft and thin copper wires were glued to the top silver electrode and the handle of the bottom silver electrode, respectively, with conductive silver paste. Finally, the entire top surface of the nanogenerator and part of the copper wires were covered with polydimethylsiloxane (PDMS) and the copper wires were further secured with Kapton tape to facilitate the subsequent polarization and performance characterization. With the top and bottom Ag electrodes of the nanogenerator connected to the negative and positive inputs, respectively, of a high-voltage power supply, the polarization of the PVDF patch was performed at 2 kV in air at room temperature for 10 min.

2.3.2. In Situ Printing of Flexible Gas Sensors. Flexible gas sensors were designed following the idea we have previously reported for sensing a nerve agent simulant (dimethyl methylphosphonate) with a chemoselective compound (selector).[7] A gas sensor was fabricated on a piece of polyimide film (Kapton HN 500, DuPont, Wilmington, Delaware, USA) and consisted of three inkjet-printed layers: an interdigitated electrode layer, a carbon nanotube layer, and a chemoselector layer. The hexafluoroisopropanol group-containing chemoselector 2-(2-hydroxy-1,1,1,3,3,3-hexafluoropropyl)-1-naphthol (a hydrogen bond donor) forms hydrogen bonds with the sensing target dimethyl methylphosphonate (a hydrogen acceptor), causing a resistance change of the carbon nanotube layer. Figure 2a shows the step-by-step fabrication process of such a gas sensor, and Figure 2b shows the basic schematic illustration of the interdigitated electrodes. Particularly, to underscore the fine feature sizes that the in situ printing system could print, the line width and spacing of the fingers of the electrodes were designed to be 70 and 125 μm, respectively. The gas

https://doi.org/10.1021/acsaelm.3c00428
ACS Appl. Electron. Mater. 2023, 5, 4157−4167

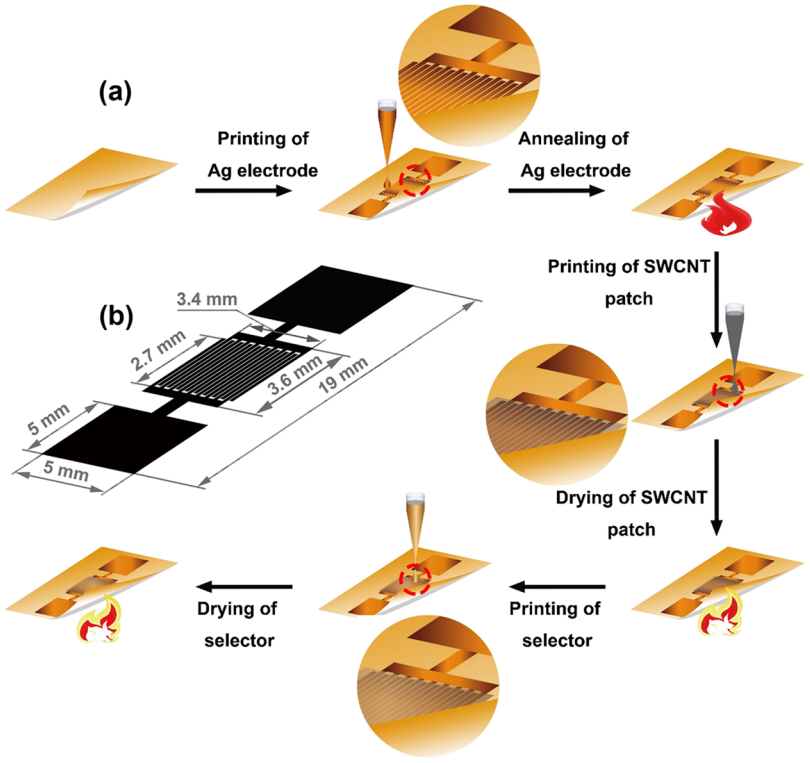

Figure 2. In situ fabrication of a flexible three-layered chemiresistive gas sensor on a Kapton polyimide film. (a) Step-by-step schematics of the fabrication process. (b) Basic schematic illustration of the interdigitated electrodes. The line width and spacing of the fingers of the electrodes, which are not shown in the illustration for tidiness purposes, are 70 and 125 μm, respectively.

sensor was printed in a similar way to that for a nanogenerator described above (Figure 1b) except that different substrates, inks, and drying processes were used. Specifically, the same silver nanoparticle ink as that used for the nanogenerator was used to print interdigitated electrodes (two passes) followed by a 150 °C/30 min annealing process performed on the hot plate. After the hot plate was cooled down to <60 °C, a DMF-based ink containing 20 μg/mL SWCNTs (IsoNanotubes-S, NanoIntegris Technologies, Inc., Boisbriand, Quebec, Canada) was printed for five passes and dried at 60 °C for 10 min on the hot plate. Finally, a DMF-based selector ink containing 10 mg/mL 2-(2-hydroxy-1,1,1,3,3,3-hexafluoropropyl)-1-naphthol (Alachua, Florida, USA) was printed (for only one pass) on top of the SWCNT layer and dried at 60 °C for 10 min on the hot plate. It is worth mentioning that both DMF-based inks (the SWCNT ink and the selector ink) had a very low viscosity of ~0.9 cP.

2.4. Printing of PVDF Patch with an Inkjet Printer. The PVDF patch is the most important component for the performance of the nanogenerator fabricated in this work. In order to compare the printing quality of the PVDF patches printed with the SonoPlot microplotter and with a conventional inkjet printer, a PVDF patch was printed on a silver patch that had been pre-printed on a Teslin synthetic paper substrate. Specifically, a silver patch (1.5 cm × 1.5 cm) was printed with the SonoPlot microplotter on the Teslin synthetic paper substrate (12 cm × 7.5 cm) by following the procedures for printing and annealing the bottom silver electrode of the nanogenerator described above. The resulting silver patch-bearing Teslin substrate was removed from the hot plate on the microplotter platen and immobilized (with heat-resistant Kapton tape) on the platen of a Fujifilm Dimatix DMP-2831 inkjet printer. A PVDF patch (1.5 cm × 1.5 cm) was printed, superposing the previously printed silver patch with the inkjet printer with a 0.5 wt % PVDF (in DMF) ink. A platen temperature of 60 °C, a 10 pL cartridge, and a drop spacing of 20 μm were used during the inkjet-printing process. In order to obtain a PVDF patch whose thickness was about the same (i.e., ~10 μm) as the PVDF patch in the nanogenerator printed with the SonoPlot microplotter printer, 80 passes had to be printed with the inkjet printer. Considering that ink diffusion is a serious concern when a large number of passes have to be inkjet-printed, printing was paused for 5 min every three passes (to dry the printed PVDF layer on the 60 °C platen) for the first 78 layers. The last two passes were then printed, followed by drying on the 60 °C platen for 10 min.

2.5. Viscosity Measurements. A Discovery HR-2 hybrid rheometer (TA Instruments, New Castle, Delaware, USA) was used to measure the viscosity of the 7 wt % PVDF ink (which was used to print the PVDF patch of the nanogenerator with the microplotter) at 25 °C, with a shear rate ranging from 0.14 to 353 s^{-1}.

2.6. Structural Characterization. Scanning electron microscopy (SEM), energy-dispersive X-ray spectroscopy (EDX), and X-ray diffraction (XRD) analyses were conducted on some components of the nanogenerator printed with the SonoPlot microplotter printer. Specifically, SEM and EDX analyses were conducted on the Teslin substrate and the top silver patch of the microplotter-printed nanogenerator, in order to reveal their micro-/nano-structural and the elemental information. XRD analyses were conducted on the bottom Ag electrode patch, the annealed but unpolarized PVDF patch, and the annealed and polarized PVDF patch, to investigate the phase transformation of the PVDF patch after the annealing and polarization processes. In order to perform these structural analyses, multiple complete or incomplete nanogenerators were fabricated with the procedures depicted in Figure 1b.

In order to compare the quality of the PVDF patch printed with the SonoPlot microplotter and that printed with a typical inkjet printer, SEM analyses were conducted on a PVDF patch printed with a Fujifilm DMP-2831 inkjet printer.

All the SEM and EDX analyses were conducted on a field emission scanning electron microscope (Leo 1530 FEG SEM, Carl Zeiss SMT Ltd., Cambridge, UK) equipped with an energy-dispersive X-ray spectrometer (INCA EDS, Oxford Instruments, Bucks, UK) at an accelerating voltage of 10 kV. Prior to any SEM or EDX analyses, an ultra-thin layer of gold−palladium was sputter-coated for 30 s with a sputter coater (Quorum Q150T ES, Quorum Technologies Ltd., East Sussex, United Kingdom) to make the samples conductive. XRD

https://doi.org/10.1021/acsaelm.3c00428
ACS Appl. Electron. Mater. 2023, 5, 4157−4167

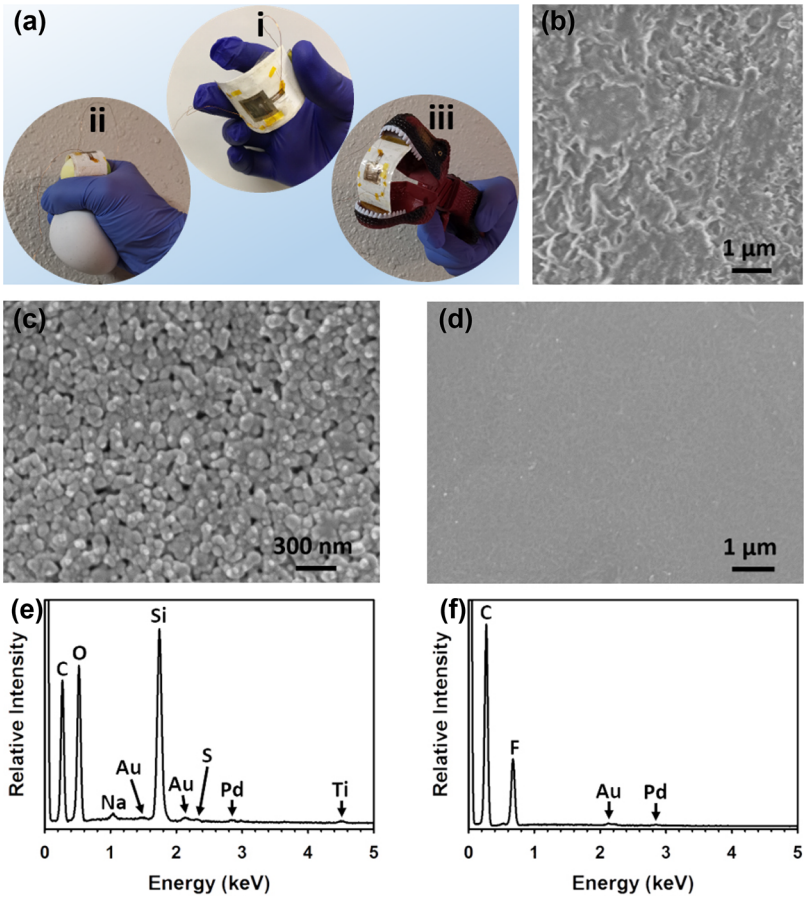

Figure 3. Optical, scanning electron microscopic and elemental analyses of a flexible PVDF-based nanogenerator. (a) Optical images of a nanogenerator being bent by human fingers (i), a squeeze ball (ii), and a dinosaur grabber toy (iii). (b), (c) and (d) Scanning electron microscopic image of the substrate (Teslin synthetic paper), the top silver electrode, and the PVDF patch, respectively, of a nanogenerator. (e) and (f) Energy-dispersive X-ray spectroscopic analyses of the specimen shown in (b) (Teslin substrate) and (d) (PVDF patch), respectively.

analyses were conducted with Cu Kα radiation using an incident beam Johannsen monochromator and an Xcelerator linear detector (X'Pert PRO Alpha-1 diffractometer, PANalytical, Almelo, The Netherlands).

2.7. Performance Characterization. In this work, performance characterization was conducted on the nanogenerator, but not on the gas sensor. The gas sensor was printed to demonstrate that the in situ printing system used to print the nanogenerator could also be used to print low-viscosity inks and fine feature sizes. Before characterizing the performance of the nanogenerator, the Teslin substrate on which the nanogenerator had been fabricated was trimmed, in such a way that the top silver patch was in the geometric center of the substrate, to dimensions of 5.5 cm × 3.5 cm. In order to increase the elasticity of the nanogenerator-bearing substrate to facilitate its continuous bending/unbending, a piece of polyethylene terephthalate (PET) film (8 cm × 2.5 cm × 0.05 cm) was attached (with double-sided Kapton tape) to the back of the Teslin substrate in such a way that the Teslin substrate and the PET film shared the same geometric center. One end of the PET film was immobilized to the stator of a home-modified programmable linear motor (LinMot USA, Inc., Lake Geneva, Wisconsin, USA) and the other end to the slider of the motor (Figure S1). The bending and unbending of the nanogenerator were realized by the computer-controlled movement of the slider. The current/voltage outputs resulting from the bending/unbending of the nanogenerator were measured with an electrometer (Model 6514, Keithley Instruments, Solon, Ohio, USA) with an internal resistance of 200 TΩ. With home-developed LabVIEW-based programs, the real-time current/voltage outputs in response to the bending/unbending of the nanogenerator were automatically recorded and schematically visualized on the computer screen.

3. RESULTS AND DISCUSSION

PVDF-based nanogenerators can be fabricated with either pure PVDF or PVDF nanocomposites. Pure PVDF was used in this work. Even though some PVDF nanocomposites, in which one or more piezoelectric fillers (such as lead zirconate titanate (PZT),[38] zinc oxide,[39,40] and barium titanate[41]) or nonpiezoelectric fillers (such as carbon nanotubes[42,43] and reduced graphene oxide[44]) are incorporated into a PVDF matrix, have enhanced piezoelectric performance,[45] pure PVDF has the following advantages over its nanocomposite counterparts: (1) Pure PVDF exhibits much better flexibility, which makes it more durable as the piezoelectric component of a device that works via cyclic bending and unbending. (2) Pure PVDF is superior in biocompatibility, long-term stability, light weight, and excellent resistance to chemical corrosion,[46] which makes it more suitable for medical textile applications and fabricating self-powered wearable electronics that can harvest energy from animal/human bodies. (3) Pure PVDF is much easier to be formulated into a printing ink than its nanocomposite counterparts. (4) A pure PVDF-based ink is much more stable than its nanocomposite counterparts.

Figure S2 shows the viscosity, as a function of shear rate, of the PVDF ink (a 7 wt % PVDF solution in DMF) used to print the PVDF patch of the nanogenerator. Apparently, the solution was a non-Newtonian fluid. Its viscosity was 232.4 cP at the lowest shear rate (0.14 1/s) used in the measurement and sharply decreased with increasing shear rate, until the shear rate reached

https://doi.org/10.1021/acsaelm.3c00428
ACS Appl. Electron. Mater. 2023, 5, 4157−4167

~20.71 1/s where the viscosity was 174.4 cP. From there on, the viscosity began to decrease slowly with increasing shear rate. At 353.38 1/s (the highest shear rate used in the measurement), the viscosity reached 159.7 cP. It has been shown that during inkjet printing, the shear rate an ink is experiencing near a nozzle is on the order of 10^5 1/s,[47,48] which is beyond the measurement range of a regular viscometer or rheometer. Consequently, we were not able to experimentally determine the viscosity of the 7 wt % PVDF solution at the shear rate that the solution experienced when it was being jetted from an inkjet nozzle. However, we loaded the PVDF solution into a 10 pL cartridge of a Fujifilm Dimatix DMP-2831 inkjet printer and found that the solution was not able to jet, which was in agreement with previous observations by Loi.[20] In contrast, this solution was dispensed very well with the microplotter used in this work, even though the shear rate applied to the solution during the microplotter printing was not known.

Figure 3a shows optical images of a flexible PVDF-based nanogenerator (on a piece of Teslin synthetic paper) fabricated with the method described above. The elasticity of the Teslin substrate was poor, but thanks to its rough surface and the excellent mechanic properties, an elastic support film (such as a PET or polyimide film) could be easily attached to its back to create the elasticity needed for bending/unbending by different devices. In Figure 3a, image (i) shows that the nanogenerator, without any back support, was bending by human fingers, while images (ii) and (iii) show that the nanogenerator, with a PET film support attached to the back of the Teslin substrate, was bending by a squeeze rubber ball and a dinosaur grabber toy, respectively. Figure 3b, c, and d show the scanning electron microscopic images of the Teslin substrate, the top silver electrode, and the PVDF patch, respectively, of a nanogenerator fabricated similarly to the one shown in Figure 3a. Since any defects in the PVDF patch would significantly affect the performance of a nanogenerator and even cause short-circuiting, we particularly inspected the entire surface, with a scanning electron microscope, of a PVDF patch printed and dried in a similar way to the PVDF patch in the nanogenerator shown in Figure 3a. Under the scanning electron microscope, the PVDF patch showed no observable defects (cracks, grooves, pits, etc.), with a typical surface morphology shown in Figure 3d. EDX analyses show that elements C, O, Na, Au, Si, S, Pd, and Ti were present in the Teslin substrate (Figure 3e), while elements C, F, Au, and Pd were present in the PVDF patch (Figure 3f). It has to be noted that the Au and Pd peaks presented in both EDX spectra (Figure 3e,f) originated from the sputter-coating of Au–Pd prior to the SEM/EDX analyses to make the specimens conductive, not from the specimens themselves. It is also worth noting that the EDX spectra of the PVDF patch (Figure 3f) show the presence of neither Ag, which originated from the bottom silver electrode right underneath the PVDF patch nor any elements from the Teslin substrate (Figure 3e). This suggests that under the accelerating voltage (10 kV) used in the EDX analyses, the PVDF patch was dense and thick enough to prevent the electron beams from reaching the underneath bottom silver electrode or the Teslin substrate, which was underneath the bottom silver electrode.

In contrast with the uniform and defect-free PVDF patch printed with the microplotter printer (Figure 3d), a PVDF patch printed with a typical inkjet printer showed nonuniformity and defects (grooves, pits, and cracks) on its surface (Figure S3). The appearance of the nonuniformity and defects in the inkjet-printed PVDF patch might be due to the following reasons: A very diluted PVDF ink (0.5 wt % in DMF) had to be used to meet the viscosity requirement of the inkjet printer, and accordingly, a large number of passes (80 passes) had to be printed. Since a 60 °C/5 min drying process had to be performed every three passes to prevent ink diffusion, the "coffee ring effect" that repeatedly took place caused the drastic nonuniformity and defects of the PVDF patch.

The piezoelectric properties of PVDF depends on its polar crystalline phases, β and γ polymorphs, with β phase exhibiting the largest electric dipole moment among all crystalline phases.[49] Approaches to induce dipole alignment for increased β phase fraction in PVDF include electric poling,[50,51] stretching,[52] thermal annealing,[53] and filler incorporation.[54] Electric poling of PVDF is traditionally performed at an elevated temperature (70–100 °C),[31,55] usually in an oil bath to prevent the formation of arcing that may damage the PVDF specimen, but has also been conducted at room temperature.[56,57] Room-temperature poling has been shown to be convenient and has commercial importance in the large-scale production of a poled material or in the fabrication of devices such as large "monolithic" transducer arrays.[56] Considering the infeasibility of introducing an oil bath to our in situ fabrication process, the PVDF patch in our nanogenerator was electrically poled at room temperature and in air.

XRD analyses was performed on some components of a PVDF-based nanogenerator that was fabricated in a similar way to the nanogenerator shown in Figure 3a, mainly to reveal phase transformation information of the PVDF patch after thermal annealing and electric poling. A 2θ range of 10–26° was chosen to highlight the peaks of the crystalline PVDF and circumvent the interferent Ag peaks originated from the bottom silver electrode patch. In this 2θ range, crystalline PVDF, but not silver, has its main XRD peaks present. The bottom Ag electrode specimen (pattern(I) in Figure 4) shows only one peak

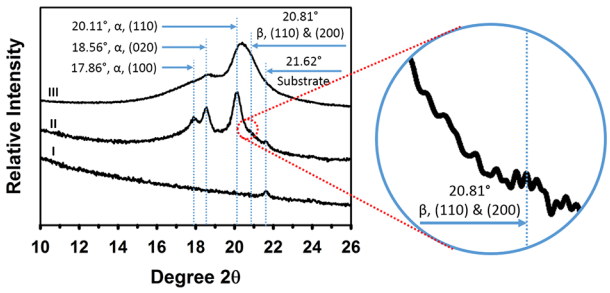

Figure 4. XRD analyses on some components of a PVDF-based nanogenerator. I, II, and III are the XRD patterns of the bottom Ag electrode patch, the annealed but unpolarized PVDF patch, and the annealed and polarized PVDF patch, respectively. The inset shows the zoomed-in image of the 20.81° PVDF β peak that is visually indistinct in pattern(II).

(21.62°), and this peak originated from the Teslin substrate. The specimen that produced pattern(II) (annealed but unpolarized PVDF patch) had been subjected to two annealing processes (i.e., 60 °C/30 min when drying the newly printed PVDF patch, and 150 °C/30 min when annealing the newly printed top Ag electrode patch). The specimen that produced pattern(III) (annealed and polarized PVDF patch) had been subjected to the same two annealing processes as the pattern(II) specimen as well as an electric poling process. Pattern(II) has a large hump (spanning from ~15 to ~23°), which originated from the amorphous phase of PVDF, a small peak at 21.62°

https://doi.org/10.1021/acsaelm.3c00428
ACS Appl. Electron. Mater. 2023, 5, 4157–4167

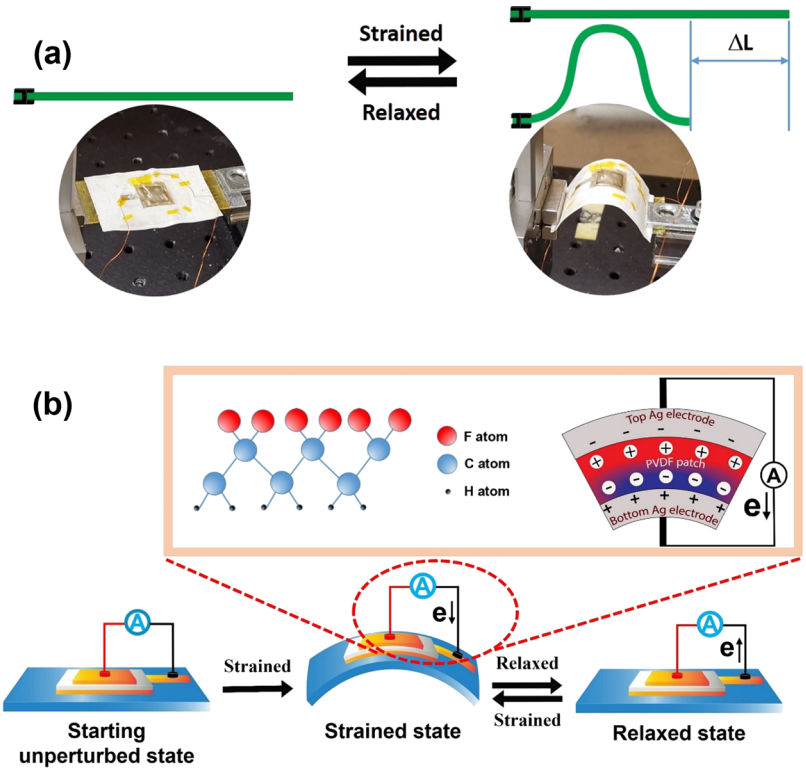

Figure 5. (a) Computer-controlled cyclic bending and unbending of a nanogenerator on a programmable linear motor. Compression ΔL is defined as the distance that the slider-immobilized end of the nanogenerator traveled. (b) Electron flow directions during current output measurements when the nanogenerator was in different states (the positive and negative inputs of the electrometer are shown in red and black, respectively). The left part of the inset shows the chemical structure of PVDF (represented in the ball-and-stick model), and the right part shows the mechanism for the electron flow directions when the nanogenerator was convexly bent.

which originated from the Teslin substrate, an indistinct peak at 20.81° (whose zoomed-in image is shown in the inset of Figure 4), and three distinct peaks (at 17.86, 18.56, and 20.11°, respectively). The indistinct peak at 20.81° matches the (110) and (200) peaks of the PVDF β phase (20.805°. ICDD PDF reference code 00-061-1404), and the three distinct peaks at 17.86, 18.56, and 20.11° match the (100), (020), and (110) peaks, respectively, of the α phase of PVDF (ICDD PDF reference code 00-061-1403). Combining all the information revealed by Figure 4 pattern(II), it can be concluded that a large portion of the annealed but unpolarized PVDF was in the α phase and only a small portion in the β phase. As shown in Figure 4 pattern(III), after the electric poling process, the two adjacent and partially overlapped α phase peaks (17.58 and 18.56°) shown in pattern(II) almost disappeared and the third α phase peak (20.11°) is broadened to the right. We suspect that the broadening of the 20.11° peak was due to the overlapping of the decreased 20.11° α phase peak and the increased 20.81° β phase peak. It has to be noted that, since the γ phase of PVDF exhibits 2θ of 18.5, 19.2, and 20.0°,[58] which are very close to the 2θ of the α (17.86, 18.56, and 20.11°) and β (20.81°) phases shown in Figure 4, it is likely that both pattern(II) and pattern(III) in Figure 4 contain the γ phase. In summary, Figure 4 suggests that under our in situ fabrication conditions, annealing alone promoted the formation of a small amount of PVDF β phase and the subsequent electric poling resulted in a significantly increased β phase fraction. As a matter of fact, for PVDF, electric poling-induced transition from the α to β phase, as confirmed by XRD and/or FTIR analyses, has been widely reported.[59−61]

In a PVDF molecule, hydrogen and fluoride atoms are partially positively and negatively charged, respectively, with respect to the carbon atoms, so that each monomer has inherent $-CH_2-CF_2-$ dipole moments. The dipoles in our printed PVDF patch were randomly oriented before the polarization. The polarization process, in which the PVDF patch was exposed to a high electric field, not only induced the formation of the β phase (pattern III of Figure 4) but also permanently aligned the dipoles.[62] With the two ends of the nanogenerator immobilized to the stator and the slider, respectively, of the linear motor, the computer-controlled back-and-forth movements of the slider made the nanogenerator exhibit bent (strained) and unbent (relaxed) states alternately (Figure 5a and Figure S1). Figure 5b shows the different states (starting unperturbed state, strained state, and relaxed state) of the nanogenerator and their corresponding electron flow when the nanogenerator was connected to an electrometer forming a short circuit. When the PVDF patch was in its starting unperturbed state, the average locations of the negative and the positive charges coincided and accordingly the molecular dipole moments in the polarized PVDF patch were in electrically neutral balance. As a result, there was no electron flow in the circuit and the short-circuit current output was zero. When the PVDF patch was bent to its convex state (strained state), its partially negatively (top side) and positively (bottom side) charged surfaces were subjected to tension and compression, respectively. As a result, the average locations of the negative and positive charges moved downward and upward, respectively, and as a result, the positive and negative charges were present on the top and bottom sides, respectively, of the PVDF patch (Figure 5b inset), which

https://doi.org/10.1021/acsaelm.3c00428
ACS Appl. Electron. Mater. 2023, 5, 4157−4167

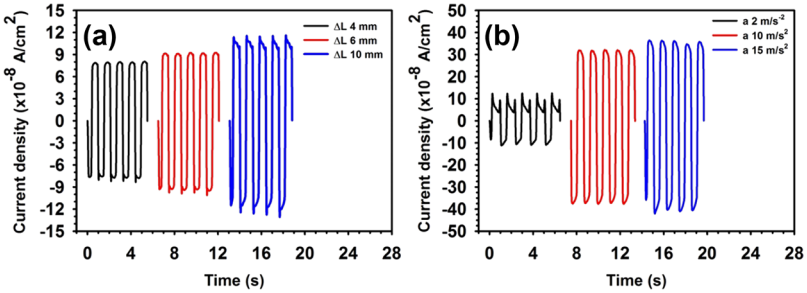

Figure 6. Negative−positive twin pulses of short-circuit current density on the PVDF patch during the cyclic bending−unbending processes with a fixed acceleration rate of 5 m/S^2 and varied compressions (a) to with a fixed compression of 15 mm and varied acceleration rates (b).

changed the charge density on both sides. By electrostatic induction, the electric charge density in both silver electrodes was redistributed, resulting in negative and positive charges on the top and bottom silver electrodes, respectively. As a result, an electric potential was formed between the two electrodes, which drove the electrons to flow from the top to the bottom silver electrode, and a negative electric current was observed if the nanogenerator was connected to an electrometer with its positive and negative inputs connected to the top and bottom silver electrodes, respectively (Figure 5b), until the electric potential between the two electrodes disappeared. When the PVDF patch was recovering from its bent (strained) state to its relaxed state, the average locations of the negative and positive charges moved upward and downward, respectively, until they coincided when the nanogenerator became completely flat. The electrons accumulated on the top silver electrode flew back to the bottom silver electrode, generating a positive current pulse. With home-developed LabVIEW-based programs, we were able to monitor the real-time changes of the short-circuit current generated in response to the bending/unbending of the nanogenerator (Supplementary Multimedia Movie). Figure 6 shows the negative−positive twin pulses of short-circuit current density during the cyclic bending−unbending processes with varied compressions (ΔL) but a fixed acceleration rate of 5 m/S^2 (Figure 6a) and with varied acceleration rates but a fixed compression of 15 mm (Figure 6b). The short-circuit current densities were calculated from the measured value of short-circuit currents divided by the effective area of the PVDF patch (1 cm^2). Under the conditions employed in the performance characterization, the maximum short-circuit current density reached ∼0.4 μA/cm^2 when the compression and the acceleration rate were 15 mm and 15 m/S^2, respectively (Figure 6b). It is worth explaining why the short-circuit densities increased with increasing accelerations. It has been reported that the short-circuit current density J_{sc} is proportional to the strain rate, as depicted by the following equation:[63]

$$J_{sc} = \bar{e}\dot{\varepsilon} \quad (1)$$

where $\bar{e}$ and $\dot{\varepsilon}$ are the effective piezoelectric constant and the strain rate, respectively, of the thin film. A higher bending acceleration results in a more rapid change in the material's shape, leading to a higher strain rate ($\dot{\varepsilon}$) and accordingly a higher short-circuit current density J_{sc}.

The microplotter printer and the in situ printing method utilized in this work are also compatible with low-viscosity inks and can be used to print fine-featured structures. Figure S4 shows the optical (Figure S4a) and SEM (Figure S4b,c) images of a fine-featured, three-layered, carbon nanotube-based chemiresistive gas sensor, printed with inks with a viscosity of as low as 0.9 cP.

To the best of our knowledge, this work demonstrated the first fully and in situ printed PVDF-based nanogenerator, which featured rapid and facile fabrication, great spatial resolution and reproducibility, minimized "coffee ring effect" and waste, and very low cost. The proof-of-concept nanogenerator described in this work was based on pure PVDF (as opposed to PVDF composites with fillers). There is still room to improve the performance of the nanogenerator fabricated with the method described in this work, including optimizing the annealing and electric poling conditions to maximize the β phase fraction in PVDF, incorporating filler nanoparticles to the PVDF matrix to enhance the piezoelectric properties, and stacking multiple nanogenerators to improve the piezoelectric responses. Also, a deeper investigation into the current nanogenerator, such as measuring the piezoelectric coefficient of PVDF patch and employing FTIR to quantitatively evaluate the phase transition of PVDF, will help fabricate a better-performing nanogenerator with the printing technology described in this work. Considering that PVDF-based flexible nanogenerators can harvest energies from a broad range of sources (such as various types of mechanic deformation, sound waves, thermal fluctuation, and air flow), the facile, rapid, and low-cost fabrication processes described in this work have industrial values. This work also provides clues for innovative designing of printers to facilitate seamless implementation of all the fabrication steps (printing, ink changing, printhead cleaning, post-printing treating, etc.) on the printers.

4. CONCLUSIONS

This work successfully attempted fully printing flexible PVDF-based nanogenerators in situ with a high-viscosity compatible microplotter printer, as an effort for rapid printing of electronic devices. The PVDF patch (the most important component of a PVDF-based nanogenerator) printed with the microplotter was densely packed and morphologically homogeneous with no observable defects, while its counterpart printed with a typical inkjet printer exhibited nonuniformity and various types of defects (such as grooves, pits, and cracks). The fabrication method employed in this work features suppressed "coffee ring effect", maximally facilitated/minimized nonprinting operations, and avoidance of the deterioration of the printing resolution and the nonuniformity/defects caused by workpiece relocation. The "coffee ring effect" when printing the piezoelectric PVDF patch was minimized via the use of a concentrated and accordingly viscous PVDF ink, with no impurities such as cosolvents, surfactants, or binders added. The nonprinting operations were minimized and facilitated via an in situ printing process in which all the steps (printing, ink changing, printhead

https://doi.org/10.1021/acsaelm.3c00428
ACS Appl. Electron. Mater. 2023, 5, 4157−4167

cleaning, post-printing treating, etc.) were seamlessly implemented on the printer. Compared with a previously reported similar work on electronic device printing, this work features rapid in situ printing, circumventing not only cartridge/printhead changes and workpiece relocation but also a number of tedious and time-consuming steps such as cartridge/printhead realignments, drop offset setting, cartridge parameter adjustment, and jetting testing. To demonstrate that the microplotter and the in situ method employed to fabricate the nanogenerator can also be employed to handle low-viscosity inks and fine feature sizes, a fine-featured, carbon nanotube-based chemiresistive gas sensor was fully printed. A PVDF-based nanogenerator fabricated in this work generated negative−positive twin pulses of short-circuit current upon cyclic bending and unbending, with a short-circuit current density magnitude up to ∼0.4 $\mu A/cm^2$. As the first-of-its-kind, the fully and in situ printed nanogenerator described in this work still has considerable room for performance improvement.

■ ASSOCIATED CONTENT

Supporting Information

The Supporting Information is available free of charge at https://pubs.acs.org/doi/10.1021/acsaelm.3c00428.

Experimental setup for the computer-controlled bending/unbending of a PVDF-based nanogenerator; viscosity of PVDF ink as a function of shear rate; scanning electron microscopic images showing the defects of a PVDF patch printed with a typical inkjet printer on the top of a silver patch that had been printed on a Teslin synthetic paper substrate; optical and SEM images of an in situ printed fine-featured chemiresistive gas sensor (PDF)

Multimedia movie showing generation of current pulses during cyclic bending/unbending of the nanogenerator (MPG)

■ AUTHOR INFORMATION

Corresponding Author

Yunnan Fang − *School of Electrical and Computer Engineering, Georgia Institute of Technology, Atlanta 30332-0245 Georgia, United States;* orcid.org/0009-0003-8491-0801; Email: yunnan.fang@mse.gatech.edu

Authors

Haiyang Zou − *School of Materials Science and Engineering, Georgia Institute of Technology, Atlanta 30318 Georgia, United States;* Present Address: College of Materials Science and Engineering, Sichuan University, Chengdu 610065, P. R. China

Song Peng − *School of Computer Science and Technology, University of Science and Technology of China, Hefei 230026, P. R. China*

Gaoya Dong − *School of Electrical and Computer Engineering, Georgia Institute of Technology, Atlanta 30332-0245 Georgia, United States;* Present Address: School of Computer and Communication Engineering, University of Science and Technology Beijing, Beijing 100083, P. R. China

Manos M. Tentzeris − *School of Electrical and Computer Engineering, Georgia Institute of Technology, Atlanta 30332-0245 Georgia, United States*

Complete contact information is available at: https://pubs.acs.org/10.1021/acsaelm.3c00428

Notes

The authors declare no competing financial interest.

■ ABBREVIATIONS

PVDF;poly(vinylidene fluoride; SWCNT;single-walled carbon nanotube; DMF;dimethylformamide; PDMS;polydimethylsiloxane

■ REFERENCES

(1) Jung, S.; Sou, A.; Banger, K.; Ko, D. H.; Chow, P. C. Y.; McNeill, C. R.; Sirringhaus, H. All-inkjet-printed, all-air-processed solar cells. *Adv. Energy Mater.* **2014**, *4*, 1400432.

(2) Shimoda, T.; Morii, K.; Seki, S.; Kiguchi, H. Inkjet printing of light-emitting polymer displays. *MRS Bull.* **2003**, *28*, 821−827.

(3) Sirringhaus, H.; Kawase, T.; Friend, R. H.; Shimoda, T.; Inbasekaran, M.; Wu, W.; Woo, E. P. High-resolution inkjet printing of all-polymer transistor circuits. *Science* **2000**, *290*, 2123−2126.

(4) Hebner, T. R.; Sturm, J. C. Local tuning of organic light-emitting diode color by dye droplet application. *Appl. Phys. Lett.* **1998**, *73*, 1775−1777.

(5) Fang, Y.; Hester, J. G. D.; deGlee, B. M.; Tuan, C.-C.; Brooke, P. D.; Le, T.; Wong, C.-P.; Tentzeris, M. M.; Sandhage, K. H. A novel, facile, layer-by-layer substrate surface modification for the fabrication of all-inkjet-printed flexible electronic devices on Kapton. *J. Mater. Chem. C* **2016**, *4*, 7052−7060.

(6) Fang, Y.; Akbari, M.; Hester, J. G. D.; Sydänheimo, L.; Ukkonen, L.; Tentzeris, M. M. Sensitivity enhancement of flexible gas sensors via conversion of inkjet-printed silver electrodes into porous gold counterparts. *Sci. Rep.* **2017**, *7*, 8988.

(7) Fang, Y.; Hester, J. G. D.; Su, W.; Chow, J. H.; Sitaraman, S. K.; Tentzeris, M. M. A bio-enabled maximally mild layer-by-layer Kapton surface modification approach for the fabrication of all-inkjet-printed flexible electronic devices. *Sci. Rep.* **2016**, *6*, 39909.

(8) Adeyeye, A.; Lynch, C.; He, X. K.; Lee, S.; Cressler, J. D.; Tentzeris, M. M. Soc, I. C. In *Fully inkjet printed 60ghz backscatter 5G RFID modules for sensing and localization in Internet of Things (IoT) and digital twins applications*, IEEE 71st electronic components and technology conference (ECTC), Electr Network, Jun 01-Jul 04; Electr Network, 2021; pp. 1193−1198, DOI: 10.1109/ECTC32696.2021.00195.

(9) He, X.; Tentzeris, M. M. In *In-package additively manufactured sensors for bend prediction and calibration of flexible phased arrays and flexible hybrid electronics*, 2021 IEEE MTT-S international microwave symposium, IEEE: 2021; pp. 327−330, DOI: 10.1109/IMS19712.2021.9574896.

(10) Cook, B. S.; Cooper, J. R.; Tentzeris, M. M. Multi-layer RF capacitors on clexible substrates utilizing inkjet printed dielectric polymers. *IEEE Microw. Wirel. Compon. Lett.* **2013**, *23*, 353−355.

(11) Su, W.; Cook, B.; Fang, Y.; Tentzeris, M. M. Fully inkjet-printed microfluidics: a solution to low-cost rapid three-dimensional microfluidics fabrication with numerous electrical and sensing applications. *Sci. Rep.* **2016**, *6*, 35111.

(12) Cook, B. S.; Fang, Y.; Kim, S.; Le, T.; Goodwin, W. B.; Sandhage, K. H.; Tentzeris, M. M. Inkjet catalyst printing and electroless copper deposition for low-cost patterned microwave passive devices on paper. *Electron. Mater. Lett.* **2013**, *9*, 669−676.

(13) Lim, J. A.; Lee, W. H.; Lee, H. S.; Lee, J. H.; Park, Y. D.; Cho, K. Self-organization of ink-jet-printed triisopropylsilylethynyl pentacene via evaporation-induced flows in a drying droplet. *Adv. Funct. Mater.* **2008**, *18*, 229−234.

(14) Still, T.; Yunker, P. J.; Yodh, A. G. Surfactant-induced Marangoni eddies alter the coffee-rings of evaporating colloidal drops. *Langmuir* **2012**, *28*, 4984−4988.

(15) Yunker, P. J.; Still, T.; Lohr, M. A.; Yodh, A. G. Suppression of the coffee-ring effect by shape-dependent capillary interactions. *Nature* **2011**, *476*, 308−311.

(16) Cui, L.; Zhang, J.; Zhang, X.; Huang, L.; Wang, Z.; Li, Y.; Gao, H.; Zhu, S.; Wang, T.; Yang, B. Suppression of the coffee ring effect by

hydrosoluble polymer additives. *ACS Appl. Mater. Interfaces* **2012**, *4*, 2775−2780.
(17) Wilkinson, J.; Tam, C.; Askounis, A.; Qi, S. Suppression of the coffee-ring effect by tailoring the viscosity of pharmaceutical sessile drops. *Colloids Surf., A* **2021**, *614*, No. 126144.
(18) Zhou, Z.; Cantu, L. R.; Chen, X.; Alexander, M. R.; Roberts, C. J.; Hague, R.; Tuck, C.; Irvine, D.; Wildman, R. High-throughput characterization of fluid properties to predict droplet ejection for three-dimensional inkjet printing formulations. *Addit. Manuf.* **2019**, *29*, No. 100792.
(19) Fortunato, M.; Cavallini, D.; De Bellis, G.; Marra, F.; Tamburrano, A.; Sarto, F.; Sarto, M. S. Phase inversion in PVDF films with enhanced piezoresponse through spin-coating and quenching. *Polymer* **2019**, *11*, 1096.
(20) Loi, A. *Inkjet printing: technique and applications for organic electronic devices*. Doctoral dissertation: University of Cagliari, 2013.
(21) Furukawa, T.; Takahashi, Y.; Nakajima, T. Recent advances in ferroelectric polymer thin films for memory applications. *Curr. Appl. Phys.* **2010**, *10*, E62−E67.
(22) Cai, R.; Kassa, H. G.; Marrani, A.; van Breemen, A. J. J. M.; Gelinck, G. H.; Nysten, B.; Hu, Z.; Jonas, A. M. An organic ferroelectric field effect transistor with poly(vinylidene fluoride-co-trifluoroethylene) nanostripes as gate dielectric. *Appl. Phys. Lett.* **2014**, *105*, 113113.
(23) Gheibi, A.; Bagherzadeh, R.; Merati, A. A.; Latifi, M. Electrical power generation from piezoelectric electrospun nanofibers membranes: electrospinning parameters optimization and effect of membranes thickness on output electrical voltage. *J. Polym. Res.* **2014**, *21*, 571.
(24) Azmi, S.; Varkiani, S.-M. H.; Latifi, M.; Bagherzadeh, R. Tuning energy harvesting devices with different layout angles to robust the mechanical-to-electrical energy conversion performance. *J. Ind. Text.* **2022**, *51*, 9000S−9016S.
(25) Gheibi, A.; Latifi, M.; Merati, A. A.; Bagherzadeh, R. Piezoelectric electrospun nanofibrous materials for self-powering wearable electronic textiles applications. *J. Polym. Res.* **2014**, *21*, 469.
(26) Kashfi, M.; Fakhri, P.; Amini, B.; Yavari, N.; Rashidi, B.; Kong, L.; Bagherzadeh, R. A novel approach to determining piezoelectric properties of nanogenerators based on PVDF nanofibers using iterative finite element simulation for walking energy harvesting. *J. Ind. Text.* **2022**, *51*, 531S−553S.
(27) Jesswein, I.; Hirth, T.; Schiestel, T. Continuous dip coating of PVDF hollow fiber membranes with PVA for humidification. *J. Membr. Sci.* **2017**, *541*, 281−290.
(28) Khan, S.; Tinku, S.; Lorenzelli, L.; Dahiya, R. S. Flexible Tactile Sensors Using Screen-Printed P(VDF-TrFE) and MWCNT/PDMS Composites. *IEEE Sens. J.* **2015**, *15*, 3146−3155.
(29) Sekine, T.; Sugano, R.; Tashiro, T.; Sato, J.; Takeda, Y.; Matsui, H.; Kumaki, D.; Dos Santos, F. D.; Miyabo, A.; Tokito, S. Fully Printed Wearable Vital Sensor for Human Pulse Rate Monitoring using Ferroelectric Polymer. *Sci. Rep.* **2018**, *8*, 4442.
(30) Chen, C.; Cai, F.; Zhu, Y.; Liao, L.; Qian, J.; Yuan, F.-G.; Zhang, N. 3D printing of electroactive PVDF thin films with high beta-phase content. *Smart Mater. Struct.* **2019**, *28*, No. 065017.
(31) Hung, S. C.; Chou, B. H.; Chang, C. Y.; Lo, C. F.; Chen, K. H.; Wang, Y. L.; Pearton, S. J.; Dabiran, A.; Chow, P. P.; Chi, G. C.; Ren, F. Minipressure sensor using AlGaN/GaN high electron mobility transistors. *Appl. Phys. Lett.* **2009**, *94*, No. 043903.
(32) Bernasconi, R.; Brovelli, S.; Viviani, P.; Soldo, M.; Giusti, D.; Magagnin, L. Piezoelectric drop-on-demand inkjet printing of high-viscosity inks. *Adv. Eng. Mater.* **2022**, *24*, 2100733.
(33) Delrot, P.; Modestino, M. A.; Gallaire, F.; Psaltis, D.; Moser, C. Inkjet printing of viscous monodisperse microdroplets by laser-induced flow focusing. *Phys. Rev. Appl.* **2016**, *6*, No. 024003.
(34) Mokrushin, A. S.; Nagornov, I. A.; Simonenko, T. L.; Simonenko, N. P.; Gorobtsov, P. Y.; Khamova, T. V.; Kopitsa, G. P.; Evzrezov, A. N.; Simonenko, E. P.; Sevastyanov, V. G.; Kuznetsov, N. T. Chemoresistive gas-sensitive ZnO/Pt nanocomposites films applied by microplotter printing with increased sensitivity to benzene and hydrogen. *Mater. Sci. Eng. B* **2021**, *271*, No. 115233.
(35) Fayez, M.; Morsi, K.; Sabry, M. N. All-ink fabrication of a TIPS-pentacene OTFT using plotter printing technique in all-air environment. In *International conference on advanced control circuits systems (ACCS) / International conference on new paradigms in electronics and information technology (PEIT)*, IEEE: Alexandria, EGYPT, 2017; pp. 319−320.
(36) Fedorov, F. S.; Simonenko, N. P.; Trouillet, V.; Volkov, I. A.; Plugin, I. A.; Rupasov, D. P.; Mokrushin, A. S.; Nagomov, I. A.; Simonenko, T. L.; Vlasov, I. S.; Simonenko, E. P.; Sevastyanov, V. G.; Kuznetsov, N. T.; Varezhnikov, A. S.; Sommer, M.; Kiselev, I.; Nasibulin, A. G.; Sysoev, V. V. Microplotter-printed on-chip combinatorial library of ink-derived multiple metal oxides as an "electronic olfaction" unit. *ACS Appl. Mater. Interfaces* **2020**, *12*, 56135−56150.
(37) Hansen, C. M. *Hansen solubility parameters: a user's handbook 2nd ed.*; CRC Press: Boca Raton, FL, USA, 2007.
(38) Bagherzadeh, R.; Abrishami, S.; Shirali, A.; Rajabzadeh, A. R. Wearable and flexible electrodes in nanogenerators for energy harvesting, tactile sensors, and electronic textiles: novel materials, recent advances, and future perspectives. *Mater. Today Sustain.* **2022**, *20*, No. 100233.
(39) Mirjalali, S.; Bagherzadeh, R.; Abrishami, S.; Asadnia, M.; Huang, S. J.; Michael, A.; Peng, S.; Wang, C.-H.; Wu, S. Multilayered electrospun/electrosprayed polyvinylidene fluoride+zinc oxide nanofiber mats with enhanced piezoelectricity. *Macromol. Mater. Eng.* **2023**, 2300009.
(40) Deng, W.; Yang, T.; Jin, L.; Yan, C.; Huang, H.; Chu, X.; Wang, Z.; Xiong, D.; Tian, G.; Gao, Y.; Zhang, H.; Yang, W. Cowpea-structured PVDF/ZnO nanofibers based flexible self-powered piezoelectric bending motion sensor towards remote control of gestures. *Nano Energy* **2019**, *55*, 516−525.
(41) Kabir, H.; Kamalidehghan, H.; Mashayekhan, S.; Bagherzadeh, R.; Bafqi, M. S. S. Hybrid fibrous (PVDF-$BaTiO_3$)/ PA-11 piezoelectric patch as an energy harvester for pacemakers. *J. Ind. Text.* **2022**, *51*, 4698S−4719S.
(42) Tang, X.-G.; Hou, M.; Ge, L.; Zou, J.; Truss, R.; Yang, W.; Yang, M.-B.; Zhu, Z.-H.; Bao, R.-Y. The preparation, structures, and properties of poly(vinylidene fluoride)/multiwall carbon nanotubes nanocomposites. *J. Appl. Polym. Sci.* **2012**, *125*, E592−E600.
(43) Lee, S.; Lim, Y. Generating Power Enhancement of Flexible PVDF Generator by Incorporation of CNTs and Surface Treatment of PEDOT:PSS Electrodes. *Macromol. Mater. Eng.* **2018**, *303*, 1700588.
(44) Lee, J.; Lim, S. Polarization behavior of polyvinylidene fluoride films with the addition of reduced graphene oxide. *J. Ind. Eng. Chem.* **2018**, *67*, 478−485.
(45) Mirjalali, S.; Varposhti, A. M.; Abrishami, S.; Bagherzadeh, R.; Asadnia, M.; Huang, S.; Peng, S.; Wang, C.-H.; Wu, S. A review on wearable electrospun polymeric piezoelectric sensors and energy harvesters. *Macromol. Mater. Eng.* **2023**, *308*, 2200442.
(46) Mohammadpourfazeli, S.; Arash, S.; Ansari, A.; Yang, S.; Mallick, K.; Bagherzadeh, R. Future prospects and recent developments of polyvinylidene fluoride (PVDF) piezoelectric polymer; fabrication methods, structure, and electro-mechanical properties. *RSC Adv.* **2022**, *13*, 370−387.
(47) Woo, K.; Jang, D.; Kim, Y.; Moon, J. Relationship between printability and rheological behavior of ink-jet conductive inks. *Ceram. Int.* **2013**, *39*, 7015−7021.
(48) Dybowska-Sarapuk, L.; Kielbasinski, K.; Arazna, A.; Futera, K.; Skalski, A.; Janczak, D.; Sloma, M.; Jakubowska, M. Efficient inkjet printing of graphene-based elements: influence of dispersing agent on ink viscosity. *Nanomaterials* **2018**, *8*, 602.
(49) Lu, L.; Ding, W.; Liu, J.; Yang, B. Flexible PVDF based piezoelectric nanogenerators. *Nano Energy* **2020**, *78*, No. 105251.
(50) Liu, Z. H.; Pan, C. T.; Lin, L. W.; Huang, J. C.; Ou, Z. Y. Direct-write PVDF nonwoven fiber fabric energy harvesters via the hollow cylindrical near-field electrospinning process. *Smart Mater. Struct.* **2014**, *23*, No. 025003.

https://doi.org/10.1021/acsaelm.3c00428
ACS Appl. Electron. Mater. 2023, 5, 4157−4167

(51) Hartono, A.; Darwin; Ramli; Satira, S.; Djamal, M.; Herman. Electric field poling 2GV/m to improve piezoelectricity of PVDF thin film. *AIP Conf. Proc.* **1719**, *2016*, No. 030021.
(52) Salimi, A.; Yousefi, A. A. FTIR studies of beta-phase crystal formation in stretched PVDF films. *Polym. Test.* **2003**, *22*, 699−704.
(53) Pan, H.; Na, B.; Lv, R.; Li, C.; Zhu, J.; Yu, Z. Polar phase formation in poly(vinylidene fluoride) induced by melt annealing. *J. Polym. Sci., Part B: Polym. Phys.* **2012**, *50*, 1433−1437.
(54) Lund, A.; Gustafsson, C.; Bertilsson, H.; Rychwalski, R. W. Enhancement of beta phase crystals formation with the use of nanofillers in PVDF films and fibres. *Compos. Sci. Technol.* **2011**, *71*, 222−229.
(55) Haghiashtiani, G.; Greminger, M. A. Fabrication, polarization, and characterization of PVDF matrix composites for integrated structural load sensing. *Smart Mater. Struct.* **2015**, *24*, No. 045038.
(56) Kenney, J. M.; Roth, S. C. Room temperature poling of poly(vinylidene fluoride) with deposited metal-electrodes. *J. Res. Natl. Bur. Stand.* **1979**, *84*, 447−453.
(57) Davis, G. T.; McKinney, J. E.; Broadhurst, M. G.; Roth, S. C. Electric-field-induced phase changes in poly(vinylidene fluoride). *J. Appl. Phys.* **1978**, *49*, 4998−5002.
(58) Ruan, L.; Yao, X.; Chang, Y.; Zhou, L.; Qin, G.; Zhang, X. Properties and applications of the β phase poly(vinylidene fluoride). *Polymers (Basel, Switz.)* **2018**, *10*, 228.
(59) Ting, Y.; Gunawan, H.; Sugondo, A.; Chiu, C. W. A New Approach of Polyvinylidene Fluoride (PVDF) Poling Method for Higher Electric Response. *Ferroelectrics* **2013**, *446*, 28−38.
(60) Ye, Y.; Jiang, Y.; Wu, Z.; Zeng, H.; Yang, Y.; Li, W. In *Characterization and ferroelectric properties of electric poled PVDF films*, 12th International Symposium on Electrets (ISE 12), Salvador, BRAZIL, Sep 11−14; Salvador, BRAZIL, 2005; pp. 132−135, DOI: 10.1109/ISE.2005.1612336.
(61) Lei, D.; Hu, N.; Wu, L.; Huang, R.; Lee, A.; Jin, Z.; Wang, Y. Preparation of efficient piezoelectric PVDF-HFP/Ni composite films by high electric field poling. *Nanotechnology Reviews* **2022**, *11*, 452−462.
(62) Shi, K.; Chai, B.; Zou, H.; Shen, P.; Sun, B.; Jiang, P.; Shi, Z.; Huang, X. Interface induced performance enhancement in flexible BaTiO3/PVDF-TrFE based piezoelectric nanogenerators. *Nano Energy* **2021**, *80*, No. 105515.
(63) Chen, J.; Oh, S. K.; Zou, H.; Shervin, S.; Wang, W.; Pouladi, S.; Zi, Y.; Wang, Z. L.; Ryou, J.-H. High-Output Lead-Free Flexible Piezoelectric Generator Using Single-Crystalline GaN Thin Film. *ACS Appl. Mater. Interfaces* **2018**, *10*, 12839−12846.

https://doi.org/10.1021/acsaelm.3c00428
ACS Appl. Electron. Mater. 2023, 5, 4157−4167